www.czasopisma.pan.pl PAN POLSKA AKADEMIA NAUK www.journals.pan.pl

Arch. Metall. Mater. **68** (2023), 4, 1667-1676

DOI: https://doi.org/10.24425/amm.2023.148335

P. GARBIEŃ[1,2], A. KOKOSZA[3], W. MAJ[2], Ł. ROGAL[1], R. CHULIST[1], K. JANUS[1], A. WÓJCIK[1], Z. ŻÓŁKIEWICZ[2], W. MAZIARZ[1*]

EFFECT OF HEAT TREATMENT ON MICROSTRUCTURE AND MECHANICAL PROPERTIES OF HIGH-CARBON AND HIGH-MANGANESE CAST STEEL SUBJECTED TO BAINITIC REACTION

The new cast steel with a chemical composition of Fe-(0.85-0.95)C-(1.50-1.60)Si-(2.40-2.60)Mn-(1.0-1.2)Al-(0.30-0.40)-Mo-(0.10-0.15)V-(1.0-1.1)Ni (all in wt.%) was investigated in aspect of formation of the multiphase microstructure leading to high strength and ductility. Two types of heat treatment technologies were developed. The first one involves softening annealing at a temperature of 650°C for 4 hours, heating up to 950°C and holding for 2 hours, and then fast cooling down to 200°C and isothermally treated for 2 hours. The second one involves homogenizing annealing at 1100°C for 6 hours, then cooling with furnace down to 950°C and holding for 2 hours, then fast cooling down to 200°C and isothermally treated for 2 hours. A unique microstructure of cast steel consisting of martensite and retained austenite plates of various thicknesses and volume fractions was obtained. Additionally, nanometric transition carbides were noticed after the above-mentioned heat treatments. This microstructure ensures high hardness, strength and plasticity (Rm = 1426 MPa and A = 9.5%), respectively, due to the fact that TWIP/TRIP processes occur during deformation related to the high volume fraction of retained austenite, which the stacking fault energy is above 15 mJ/m^{-2} resulting from the chemical composition of the investigated cast steel.

Keywords: Cast steel; multiphase microstructure; TEM; mechanical properties

1. Introduction

Over the last decades, several studies have been focused on the development of new bainitic steels with a composition characterized by an interesting combination of tensile strength, ductility, and impact toughness [1-3]. These new steels can reach ultimate tensile strength (UTS) levels around 2 GPa and total elongations above 20%. These steel grades, belonging to the 3rd generation of the advanced high-strength steels (AHSS), are characterised by a multiphase microstructure composed of carbide-free bainite with a significant volume fraction of stable carbon enriched retained austenite (RA) and martensite [4]. Such microstructure is obtained after austempering treatments. It consists of an austenitizing stage followed by rapid quenching and isothermal holding in a hot bath at a temperature between the bainite start (B_s) and martensite start (M_s) temperatures for a predetermined interval of time [5-7]. According to the literature [8], carbide-free bainitic steels are promising materials also for applications in which high wear resistance is required. So far, the formation of this type of microstructure or nanostructured bainite in castings is very rarely presented in literature [9-12]. Therefore, there is a strong need to undertake this type of research, which may be a breakthrough in the foundry industry. In Ref. [9], authors attempted to obtain a nanostructured bainite in cast steel with a carbon content of 0.76 wt.% postulating that it is possible to select the optimal heat treatment to obtain a nanobainitic microstructure. The microstructure observed for selected temperatures of low-temperature isothermal annealing were identical to those occurring in wrought materials. However, there was differences in mechanical properties, probably caused by the inherent microsegregation characteristic of castings. Moreover, in terms of future industrial implementations of this type of cast steel, the annealing time was twice as long compared to the generally used one, but it did not lead to a significant improvement of mechanical properties. Therefore, it can be concluded that another type of heat treatment is required to be used before low-temperature isothermal treatment. In the works [10,11], the authors attempted to determine the influence of dendritic microsegregation on the bainitic transformation in high-carbon steels with a high silicon content. A heterogeneous distribution of silicon, manganese

[1] INSTITUTE OF METALLURGY AND MATERIALS SCIENCE, POLISH ACADEMY OF SCIENCES, 25 REYMONTA STR., 30-059, KRAKÓW, POLAND
[2] SPECODLEW SP.Z O.O. ROTMISTRZA WITOLDA PILECKIEGO 3 STR., 32-050 SKAWINA, POLAND
[3] AGH UNIVERSITY OF KRAKOW, FACULTY OF METALS ENGINEERING AND INDUSTRIAL COMPUTER SCIENCE, AL. MICKIEWICZA 30, 30-059 KRAKOW, POLAND
* Corresponding author: w.maziarz@imim.pl

and chromium concentrations was found, related to dendritic microsegregation occurring during casting, which strongly affects the final microstructure achieved after isothermal treatment at temperatures of 280, 330 and 380°C. Tensile strength tests showed that the ultra-fine microstructure obtained during isothermal transformation at 280°C results in a strength of 1.8 GPa but with limited plasticity of approximately 2%. It is evident that one of the main reasons for the inappropriate balance between strength and plasticity in cast steels subjected to isothermal bainitic transformation is the occurrence of segregation of the chemical composition. Therefore, design work should be carried out towards both the modification of the chemical composition of cast steels and the casting followed by heat treatment technology. Another interesting investigations on the microstructure and properties of cast steel subjected to isothermal heat treatment resulting in the formation of carbide-free nanobainite was presented in Ref. [12]. For four different isothermal treatment times at 250°C, 55, 75, 85 and 100% progress of bainitic transformation was obtained, respectively. It was also interesting that in samples with a bainitic transformation of 55 and 75%, the transformation of retained austenite into martensite occurred when cooling to room temperature. Despite the obtaining of a nanobainitic microstructure in the castings similar to that in plastically processed steels, the authors also observed the occurrence of dendritic segregation and cementite precipitates related to the pearlite transformation. The softening treatment applied at a temperature of 680°C allowed for a partial reduction in segregation as a result of spheroidization of carbides, as well as a reduction in hardness, which allowed for an increase in the machinability of the tested cast steel. Similarly to the works [9-11], the authors achieved high strength properties of the designed cast steels, but with low plasticity. It can be seen that, while maintaining an appropriate heat treatment regime and for selected cast steel compositions, it is possible to obtain a nanobainitic microstructure in the similar to that found in steels and with high strength values, but the improvement of their plasticity and elimination of dendritic segregation remain an unsolved problem.

Therefore, this work continues research on modern cast steels characterized by multiphase microstructure what is still a major scientific and industrial challenge that is worth undertaking in terms of future applications.

2. Experimental

The chemical composition of investigated cast steel was as follow: 0.85-0.95% C; 1.50-1.60% Si; 2.40-2.60% Mn; 1.0-1.2% Al, 0.30-0.40% Mo; 0.10-0.15% V, 1.0-1.1% Ni (all in wt.%). The casting process of investigated cast steel was conducted using of the equipment of the production company. Therefore, one casting process concerned a cast steel weight of 160 kg. The induction melted cast steel with 1560°C temperature was poured to the ceramic mould covered with 7-8 coatings of water binder having 960°C. Then mould was cooling down to the room temperature in tunnel furnace with the constant cooling rate. It was assumed that the crystallization rate in industrial conditions is almost constant for a cross-section of the cast. The samples for investigations were taken out from the central part of the cast and prepared by the machining of parts of casts to the cylindrical shape with a diameter of Ø10 mm and a height of 100 mm. Before carrying out the appropriate heat treatment, the samples were subjected to chemical analysis by the Glow-discharge optical emission spectroscopy (GDOES) using of Foundry Master Xpert 52 spectrometer. For each sample, two measurements at two opposite sides were performed to check their chemical homogeneity. An example of such analysis is presented in Fig. 1. This procedure allowed to ensure that all used samples in further investigations were characterised by identical chemical composition.

Dilatometric analysis was used to determine the initial heat treatment parameters. During this research, a sample of the investigated cast steel with dimensions of 3×10 mm, in as-delivered state, was heated to 1200°C with a rate of 0.05°C/s in the L78 R.I.T.A. dilatometer. While heating the samples, the relative elongation of the samples ($\Delta L/L_0$) was recorded as a function of temperature (T). After differentiating this relationship, critical temperatures were determined. A similar test was performed for a sample that before heating to 1200°C was initially annealed at 650°C. The critical temperatures determined in this way were:

- for the sample as delivered (after casting): Ac_{1s} = 720°C, Ac_{1f} = 745°C, Ac_{cm} = 855°C,
- for the sample after annealing at 650°C: Ac_{1s} = 705°C, Ac_{1f} = 750°C, Ac_{cm} = 855°C.

Based on these temperatures, it was possible to determine the target temperature for basic austenitization. Meanwhile, the temperature of isothermal holding in the bainitic transformation range was selected based on the knowledge of the M_s temperature (51°C), which was determined on the basis of simulations with the JMatPro software.

Taking into account a dilatometric analysis, JMatPro simulations, as well as the company's capabilities and from the economic point of view, two different heat treatments leading to the achievement of outstanding properties of the investigated cast steels were proposed:

1. Homogenization annealing at 1100°C for 6 hours, cooling down to the austenitization temperature of 950°C and holding in this temperature for 2 hours, then fast cooling to 200°C and isothermal annealing at this temperature for 2 hours.
2. Softening annealing at 650°C for 4 hours then, heating up to austenitization temperature of 950°C and holding in this temperature for 2 hours, then fast cooling to 200°C and isothermal annealing at this temperature for 2 hours.

One can see that these two variants of heat treatment differ only in the first step. In the first case, there is homogenization annealing at 1100°C for 6 hours, during which the diffusion processes enabling the elimination of the dendritic segregation (always present in casts) were examined. The second one has a soft annealing at 650°C for 4 hours, during which we expect to obtain more stable, equilibrium microstructure of perlite with spheroids of cementite before the austenitization process, which

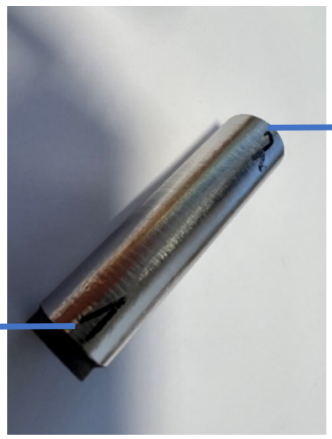

Analyse 1								
Chemical element	Fe	C	Si	Mn	P	S	Cr	Ni
Average	92.3	0.855	1.42	2.46	0.0231	0.0201	0.0203	1.07
Chemical element	Mo	Cu	V	W	Ti	N	Al	Co
Average	0.375	0.0420	0.129	0.0054	0.0429	0.0591	0.965	0.0087
Chemical element	Nb	Pb	Sn	B	Ca	Se	Sb	Ta
Average	0.0315	0.0094	0.0142	0.0002	0.0010	0.0115	0.0052	0.180

Analyse 2								
Chemical element	Fe	C	Si	Mn	P	S	Cr	Ni
Average	91.9	0.860	1.43	2.59	0.0241	0.0220	0.0218	1.10
Chemical element	Mo	Cu	V	W	Ti	N	Al	Co
Average	0.375	0.0429	0.129	0.0276	0.0465	0.0561	0.981	0.0173
Chemical element	Nb	Pb	Sn	B	Ca	Se	Sb	Ta
Average	0.0366	0.0103	0.0125	<0.0002	0.0015	0.0093	0.0091	>0.180

Fig. 1. An example of GDS chemical analysis performed in two places of as cast cylindrical sample

finally allows for an increase in the machinability of the cast steel. For simplicity, samples will now be labelled as CS1100 and CS650 according to applied heat treatment. In order to prevent the oxidation and decarbonisation of the surface of samples the heat treatments were conduct in protected atmosphere of nitrogen which was deliver into furnace in quantity of 7 m^3/h. The wide scale microstructure investigations were performed after heat treatment process. Optical Light Microscopy (LM) was applied for etched samples in order to reveal the main constituents of the microstructure. The samples were mechanically grinded using silicon carbide paper up to 7000 grit and polished using alumina suspension until the complete disappearance of scratches. Etching process of the samples surface was performed using of solution of 3% nitric acid in ethanol (Nital). Keyence digital microscope was used for microstructural observations. Detailed microstructural observations and crystal structure analysis were carried out by Tecnai G2 200 kV scanning /transmission electron microscope (S/TEM) equipped with EDX detector system and Themis 200 G3 with Cs corrector and high efficiency Super-X EDS Detection System for chemical analysis. Thin foils for TEM observations were prepared with a TenuPol-5 double jet electropolisher using an electrolyte of nitric acid (70%) and methanol (30%) at –25°C. The crystal structure, lattice parameter of phases and their volume fraction in investigated samples were determined using of X-ray diffraction of high-energy synchrotron radiation (87.1 keV) in transmission geometry using the HZG materials science beamline P07B at DESY in Hamburg, German. Mechanical properties of investigated samples were determined using of hardness measurement and tensile test.

3. Results and discussion

The phase analysis of samples after two different heat treatments was performed using diffraction of high energy synchrotron radiation. Fig. 2 shows the high-energy X-ray diffraction patterns recorded at room temperature. For both cases, all visible peaks can be attributed to two phases α' martensite and γ austenite phases. However, in the two theta range between 3.75-4.25, significant differences in shape and intensities of peaks can be observed. This indicates that the volume fraction of martensite and austenite, their lattice parameters and carbon concentrations are different due to application of two different heat treatments. By use of the fitting procedure of peaks and their deconvolution, it was possible to calculate the volume fraction of austenite and martensite, lattice parameter of austenite, carbon concentration in austenite, tetragonality of α' martensite as well as the stacking fault energy (SFE) of the austenite. The volume

fraction of austenite and martensite was clearly different for both applied heat treatments. In the case of sample CS1100, the volume fraction of austenite and martensite was found to be 58.8 and 41.2%, respectively, whereas for CS650 sample equals 67.8 and 32.2%. These results indicate that annealing of samples at the higher temperature prior to austenitization promotes the formation of a larger amount of martensite after quenching and isothermal annealing. The carbon concentration of retained austenite in the tested steel was calculated using Eq. 1 [13]

$$a_0 = 3.5780 + 0.033C_\gamma \tag{1}$$

where a_0 is the austenite lattice parameter in Angstroms and C_γ is the weight percent of the carbon in the retained austenite.

The lattice parameters of retained austenite were calculated and are equal 3.6103 Å and 3.6023 Å for CS1100 and CS650, samples respectively. Based on these results, the carbon concentration of retained austenite (c_γ) was determined as 0.98 wt.% and 0.74 wt.% in the case of specimens CS1100 and CS650, respectively. The tetragonality of the martensite was calculated according to reference [14], while the carbon concentration in the martensite was determined using Eq. 2 [15] in both samples:

$$C_a = \frac{0.28674\left(\frac{c}{a} - 1\right)}{0.0115 + 0.00124\frac{c}{a}} + 0.18 \tag{2}$$

In the case of martensite, the lattice parameters, tetragonality (c_a/a_a), and carbon concentration of martensite (C_a) were determined. Based on lattice parameters, the (c_a/a_a) is 1.0408 and 1.0336 in the case of CS1100 and CS650 samples, respectively. Determination of the tetragonality of martensite allowed for the calculation of the carbon concentration within. It was observed that the carbon concentration of martensite is 1.09 wt.% and 0.93 wt.% for specimens CS1100 and CS650, respectively and it is generally higher than in retained austenite. For better visibility all calculated parameters from high energy synchrotron diffraction were collected in TABLE 1.

Most steels contain the retained austenite after different heat treatment, therefore the mechanical properties should also depend on its deformation mechanism. Moreover, in our case after isothermal annealing at 200°C for 2 hours the retained austenite constitutes a significant volume fraction and even is a predominated phase for both investigated cast steels. Therefore, an increase of strength and ductility can be expected when the samples are deformed due to the twinning induced plasticity (TWIP) or dislocation glide in austenite.

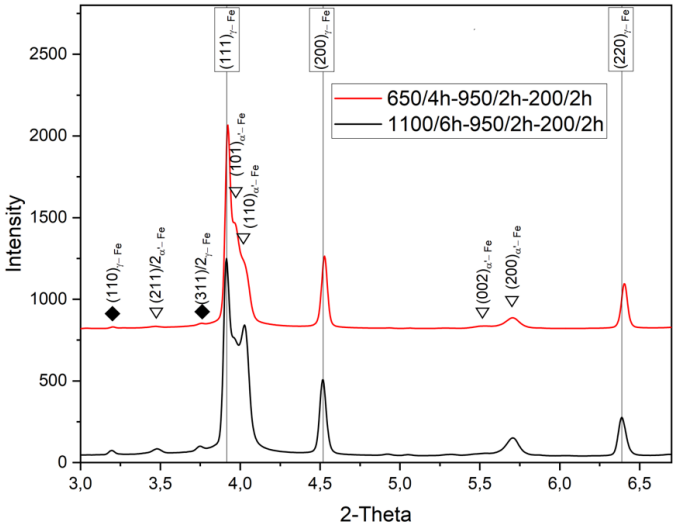

Fig. 2. High-energy X-ray synchrotron diffraction patterns for samples after two different heat treatment procedures

The deformation mechanisms and mechanical properties of face-centered cubic (*fcc*) metals are strongly related to their stacking fault energy (SFE) γ_{SFE} [16], which is the most crucial nucleation parameter determining whether twinning, martensitic transformation or dislocation glide alone will occur during the deformation of the material. Twinning is reported to occur at stacking fault energies roughly $18 \leq \gamma_{SFE} \leq 45$ mJ m^{-2}. At γ_{SFE} values <18 mJ generally formation of ε or α' martensite occurs, becomes the favoured transformation mechanism that affects the further deformation of the material. For $\gamma_{SFE} > 45$ mJm^{-2}, plasticity and strain hardening are controlled solely by the glide of dislocations. The γ_{SFE} was calculated for the composition presented in Fig. 1 equal 22 mJ/m^{-2} and is connected with a high concentration of Mn and Al. This indicates that during plastic deformation the retained austenite can be deformed by TWIP (twinning-induced transformation) mechanism and increase the strength and ductility.

In order to determine the morphology of austenite and martensite as well as crystallographic relationships between them, a wide spectrum of microscopy investigations was applied. Firstly a light microscopy microstructure observations were performed in order to characterise the microstructure at low magnifications with the aim to show the chemical segregation and grain size. Fig. 3 presents the set of microstructures for samples after both heat treatment processes recorded at different magnifications. At the lowest magnifications (upper row) a significant differences of microstructure can be recognised be-

TABLE 1

Volume fraction, lattice parameters and carbon concentration in austenite and martensite calculated by use of high-energy X-ray diffraction

Sample	V_γ [vol.%]	a_γ [Å]	C_γ [wt.%]	V_α [vol.%]	a_α [Å]	c_α [Å]	$\frac{c_\alpha}{a_\alpha}$	C_α [wt.%]
CS1100	58.8	3.6103	0.98	41.2	2.85816	2.9746	1.041	1.09
CS650	67.8	3.6023	0.74	32.2	2.8592	2.9554	1.034	0.93

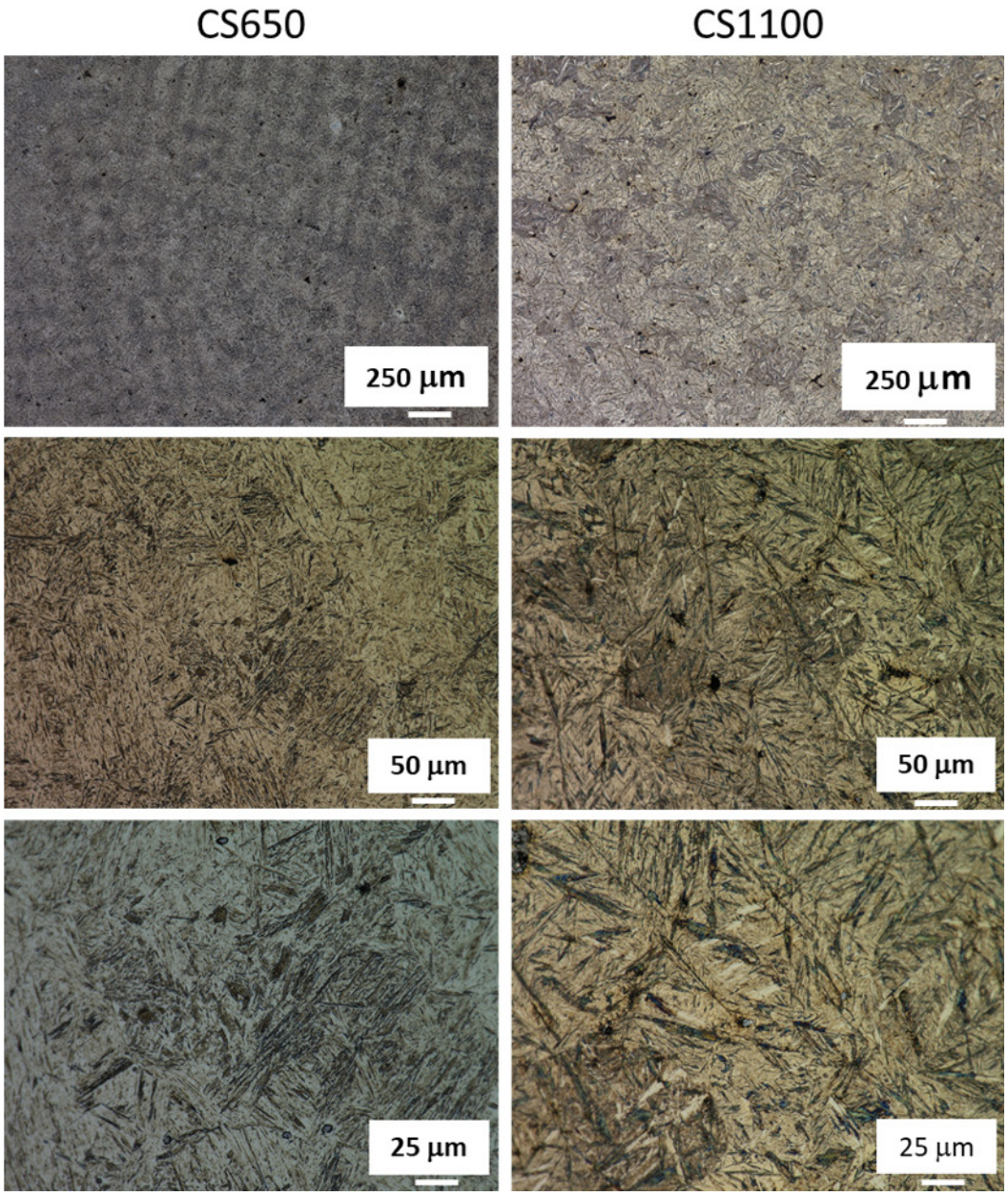

Fig. 3. Set of microstructures of samples after both heat treatment processes recorded at different magnifications

tween two applied heat treatments. In the case of sample CS650, a dendritic microstructure is visible while in the case of CS1100 the granular one. Although there is a dendritic microstructure, in this case it is relatively uniform with uniform areas of dendrite arms and interdendritic areas. Therefore, it can be assumed that both softening annealing and austenitization at a temperature of 950°C lead to some level of microstructural uniformity. In the case of sample CS1100 one can see the granular microstructure with irregular grains of the size of about 300 mm. Thus, it can be concluded that at least in the observed area combined high temperature homogenization annealing and austenitization led to a significant reduction of dendritic segregation. The type of microstructure obtained during austenitization just before fast cooling down to bainitic reaction temperature strongly influences the final bainitic microstructure. The dendritic microstructure subjected to bainitic reaction was presented in Ref. [17]. The authors found that transformation starts in the dendritic zones depleted with Mn and then expands to the interdendritic ones.

Since Mn reduces the C activity, the interdendritic areas with a higher Mn concentration are enriched with C, and thus, these zones contain a greater amount of retained austenite plus martensite, resulting in a heterogeneous microstructure. Finally this shift of the M_s temperature toward the higher temperatures range promoting the formation of a bigger amount of retained austenite and the presence of martensite in the final microstructure. Such type of microstructure may be observed in Fig. 3 at the higher magnification for CS650 sample. In case of CS1100 sample microstructure recorded at higher magnification is characterised by the bigger grains of prior austenite influencing the increase of M_s temperature [18,19] and higher volume fraction of martensite. Summarising, microstructure observations of

samples using LM allowed to conclude that both cases of heat treatment of investigated cast steel applied prior austenitization leads to an increase of M_s temperature and finally formation of two phase structure of austenite plus martensite. The effect of prior martensite on bainite transformation in nanobainite steel was investigated by W. Gong et. al. [20]. What is worth to notice, they used for investigations of low alloy steel with carbon (0.79C), manganese (1.98Mn) and silicon (1.51Si) content close to our case (all in wt.%). The samples were prepared by vacuum induction melting while ingot was homogenized at 1200°C for 4 hours, what is also similar to the investigated CS1100 cast steel. Finally, the samples were hot rolled and applied for two series of heat treatment processes (a) the direct isothermal transformation (DIT) process and (b) the quenching and bainite transformation (QBT) process. In QBT, a specimen was austenitized at 900°C for 20 min before rapid cooling to 110 or 300°C (below M_s), then heated up to 250 or 300°C for isothermal holding and finally cooled down to room temperature. There is no partial quenching process for DIT treatment, and a specimen was cooled from 900°C directly to 250°C or 300°C for isothermal bainite transformation. Based on detailed studies using in-situ neutron diffraction measurements, scanning electron microscopy and electron backscatter diffraction observations, authors found that prior martensite transformation accelerate the subsequent nanobainite transformation. Bainitic lathes formed adjacent to a pre-existing martensite plate exhibited an almost identical orientation. Dislocations introduced in austenite due to stress relaxation of transformation strains are believed to assist bainite transformation accompanying variant selection. Neutron diffraction profiles of austenite were found to show symmetric broadening with martensite transformation whereas nonsymmetric broadening occurred with nanobainite transformation, indicating the generation of two populations of austenite. Taking into account our findings concerning the increase of M_s temperature due to dendritic inhomogeneities and prior austenite grain size increase as well as results in [20] we may expect that in our cast steel after DIT process also bainitic transformation at 200°C occurs and some part of the microstructure can include a nanobainte. In order to determine a morphology of austenite and martensite and crystallographic orientation between them detailed TEM microstructure investigations were made. Also by the use of the most sophisticated Super-X EDS system in TEM an accurate chemical analyse of particular phases, was performed. This higher efficiency EDS detection systems enable fast compositional analysis with below nanometer resolution. Additionally, the Super-X Detection System features 4 SDDs detectors for substantially enhanced sensitivity, which is critical for trace element detection for example carbon. Fig. 4 presents a result of the microchemical analysis of CS650 sample performed in TEM using the Super-X EDS system.

One can see the HAADF microstructure and corresponding elemental maps, as well as results of quantitative chemical analyses performed in the indicated areas. Generally, it can be seen that the distribution of all elements present in cast steel is uniform and does not depend on any visible differences in the HAADF microstructure. Only nanometric-sized longitudinal precipitates can be seen, enriched in V and Mo and depleted in Fe. Quantitative chemical analysis performed in the marked areas indicates slight carbon fluctuations in the examined areas, but they are on the verge of measurement error. In general, it can be said that this content is about 1 wt.%, which is consistent with the nominal chemical composition of cast steel, but it will not allow to clearly determine what type of phase we are dealing with (austenite or martensite plate), which should differ in carbon content according to results obtained using synchrotron radiation diffraction (TABLE 1). Therefore, other TEM techniques, i.e. selected area electron diffraction (SAED) and dark field (DF) observations, can only solve this problem. Interestingly, most of the analysed elements have concentrations similar to the nominal ones, except for manganese, which is higher even if we take into account the measurement error. Fig. 5 presents HAADF microstructure and results of chemical analyse of sample CS1100. The same phenomena are visible as in the case of the CS1100 sample, i.e. uniform distribution of all cast steel alloying elements and occasional occurrence of nanometric precipitates enriched in V and Mo and depleted in Fe. However, in this case, these precipitates can be recognised as carbides because of a slight but significant increase of the carbon signal occurs in

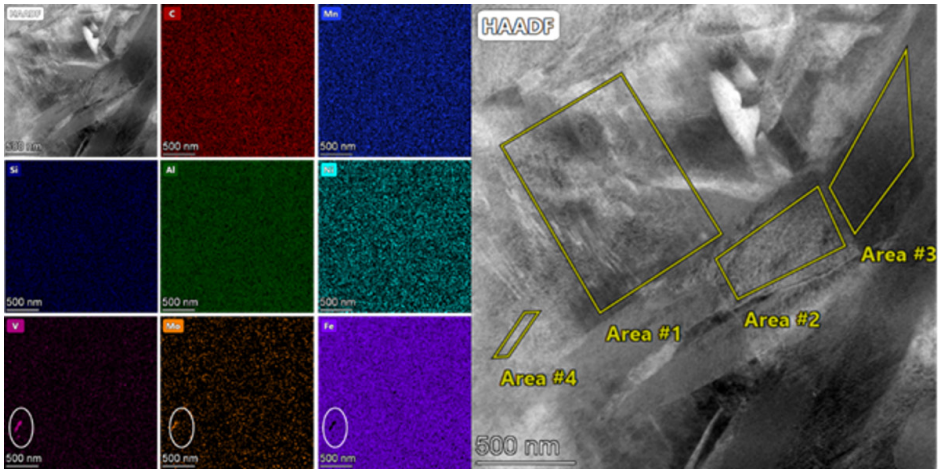

Area 1

Element	Mass Fraction (%)	Mass Error (%)
C K	1.36	0.17
Al K	0.53	0.12
Si K	1.05	0.24
V K	0.10	0.02
Mn K	3.99	0.72
Fe K	balance	-
Ni K	0.98	0.18
Mo K	0.19	0.04

Area 3

Element	Mass Fraction (%)	Mass Error (%)
C K	1.41	0.17
Al K	0.58	0.14
Si K	1.09	0.25
V K	0.10	0.02
Mn K	3.97	0.72
Fe K	balance	-
Ni K	0.99	0.18
Mo K	0.44	0.09

Area 2

Element	Mass Fraction (%)	Mass Error (%)
C K	1.34	0.16
Al K	0.56	0.13
Si K	1.14	0.26
V K	0.14	0.03
Mn K	3.99	0.72
Fe K	91.43	16.49
Ni K	0.97	0.16
Mo K	0.43	0.08

Area 4

Element	Mass Fraction (%)	Mass Error (%)
C K	1.49	0.18
Al K	0.76	0.18
Si K	1.06	0.24
V K	3.41	0.60
Mn K	3.62	0.74
Fe K	balance	-
Ni K	0.99	0.18
Mo K	2.89	0.59

Fig. 4. HAADF microstructure and corresponding of elemental maps (wt.%) of sample CS650 performed in TEM using of Super-X EDS system

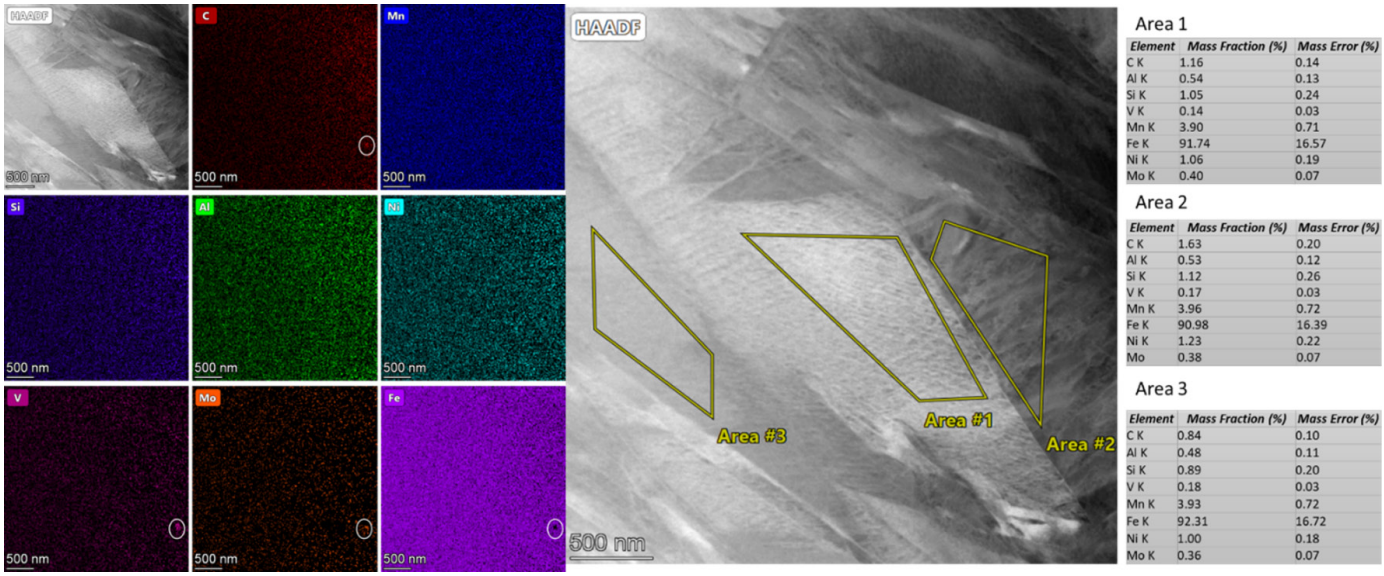

Fig. 5. HAADF microstructure and corresponding of elemental maps (wt.%) of sample CS1100 performed in TEM using of Super-X EDS system

this area. Quantitative analysis performed in the marked areas indicates that this samples is also enriched with manganese to approximately 3.9 wt.%, which may be evidence of a change in the nominal composition of the cast steel and should be taken into account in further investigations.

Greater fluctuations in carbon concentration are also visible, which may indicate that plates with a lower content are martensite, and those with a higher content represents austenite. It is also visible that these plates differs in morphology and contrast. In order to confirm these insights, observations were carried out using bright field (BF), dark field (DF) and selected area electron diffraction (SAED). The set of BF and DF microstructures and the corresponding SAED images taken for CS650 and CS1100 samples are shown in Figs. 6 and 7, respectively. In both cases, a two-phase austenitic-martensitic microstructure is visible, which is confirmed by electron diffractions. Each of them shows two martensite sublattices with the zone axis orientations $[010]_M$ and $[111]_M$, respectively, and one austenite with the zone axis orientation $[111]_A$. The selection of reflections from the appropriate austenite and martensite planes was made so that the microstructure components from only one phase were visible in the DF microstructures.

Therefore, it can be concluded that the martensite plates for both heat treatment variants are much wider than those of

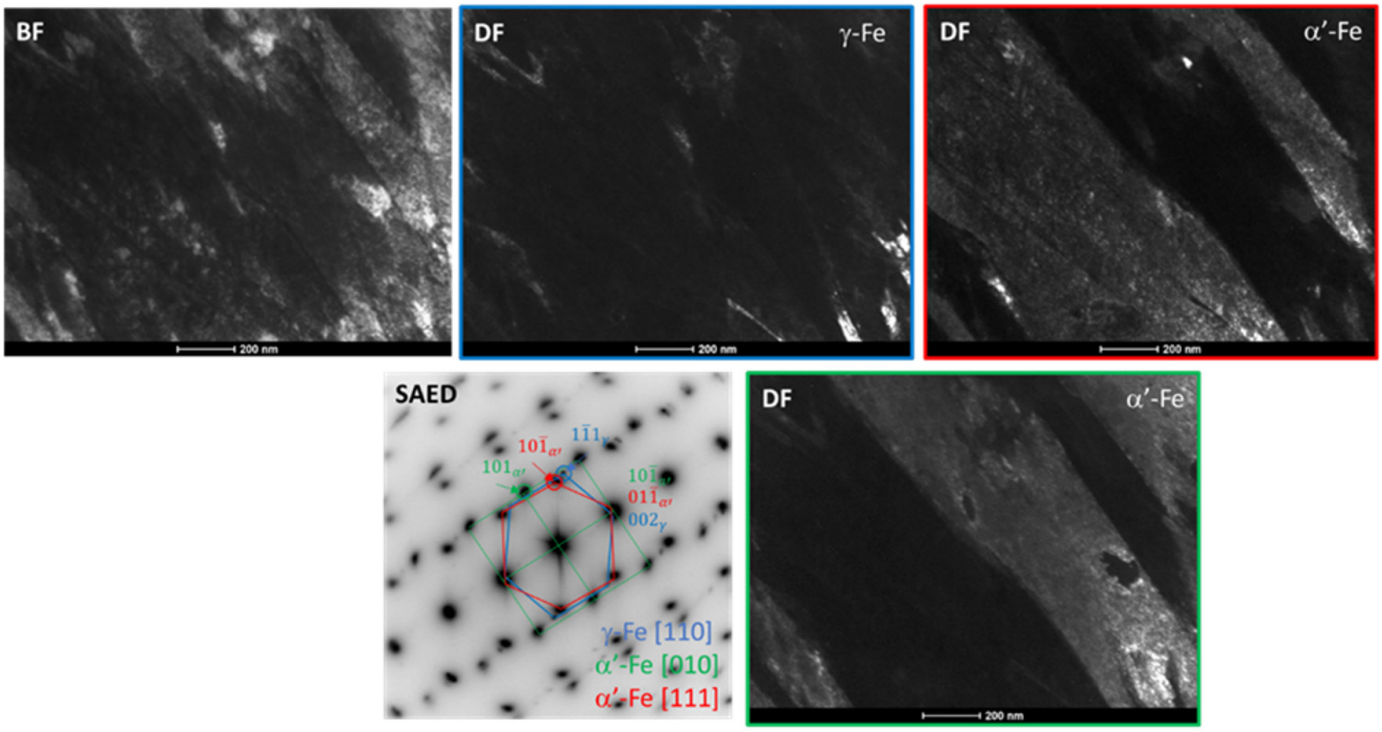

Fig. 6. The set of BF and DF microstructures and the corresponding SAED images taken for CS650 sample

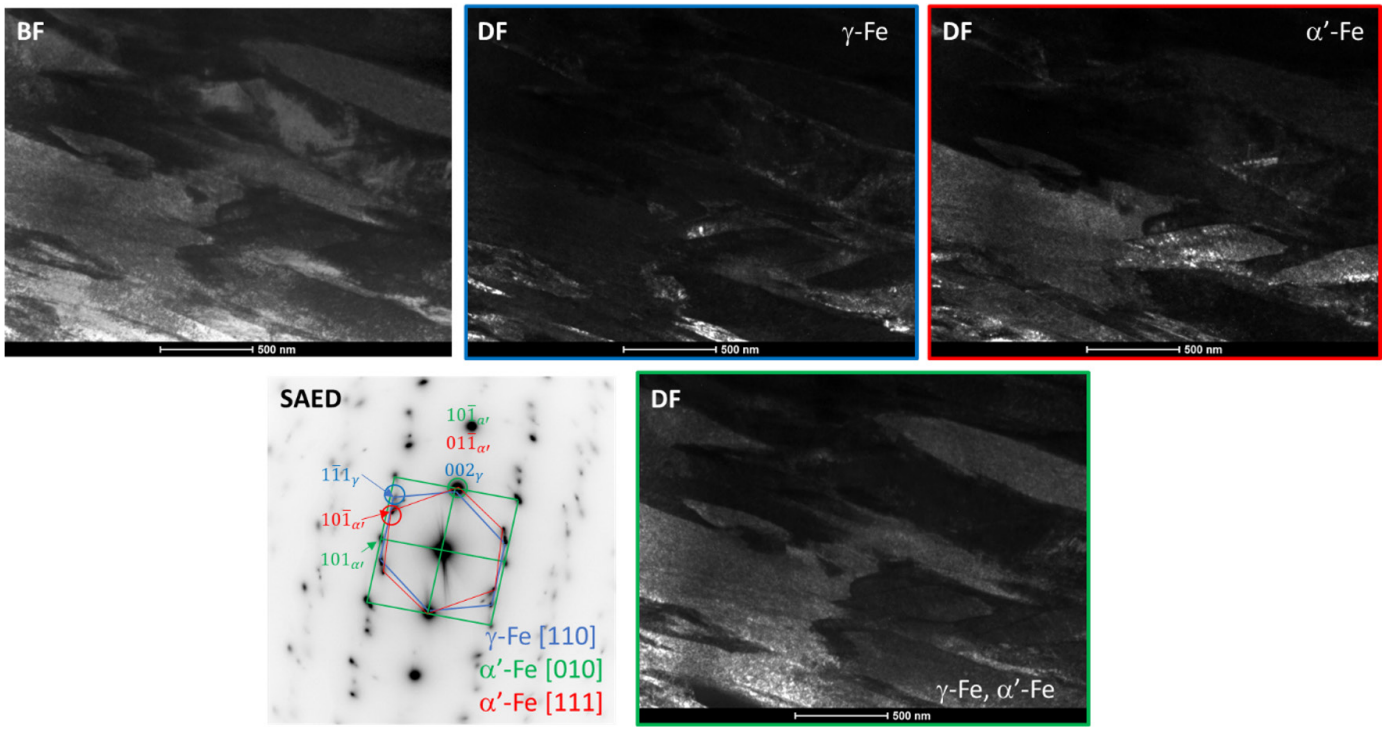

Fig. 7. The set of BF and DF microstructures and the corresponding SAED images taken for CS1100 sample

austenite and their width ranges from 200 to 500 nm, while the width of the austenite plates ranges from several to 50 nm for CS650 sample and from several dozen up to 200 nm for CS1100. It is possible that the main reason for these differences is related to the growth of the prior austenite grain during annealing at a temperature of 1100°C. However, in the case of CS650 sample, it should be remembered that there may be a different microstructure (morphology) of martensite and austenite in both dendritic and inter-dendritic areas, as shown in Fig. 3. Additionally, based on the obtained diffraction patterns, it is visible that in both cases there is a crystallographic relationship between austenite and martensite of the Kurdjumov-Sachs type $\{111\}_\gamma // (011)_{\alpha'}$ and $\bar{1}01_\gamma // \bar{1}\bar{1}1_{\alpha'}$ respectively for blue and red orientations shown in the DF images in Figs. 6 and 7. As presented above, EDS chemical analysis showed the presence of nanometric carbide precipitates. Detailed microstructural analysis using high-resolution transmission electron microscopy (HREM) allowed the detection and description of these carbides. Fig. 8 shows the BF microstructure and the corresponding electron diffraction, which can be fitted to the α' martensitic phase with the [111] zone axis orientation, observed in the sample CS1100.

However, for this zone axis of α' phase, the angle between all {110} diffraction spots should differs from 60°, since martensite has a tetragonal structure. However, precise measurements using TIA software indicated that that are equal exactly to 60° what suggests that this phase can be consider as bainitic ferrite α_{bf} with the *bcc* regular crystal structure. This partially proofs previous considerations about the increase of M_s temperature and formation of bainite structure in the investigated cast steel. The BF image show additional microstructural effects in the form of nanometric bands, and the diffraction patterns show additional weak reflections (indicated by the arrows) located closer to the transmitted beam (central reflection), indicating the presence of an additional phase. Therefore, an attempt was

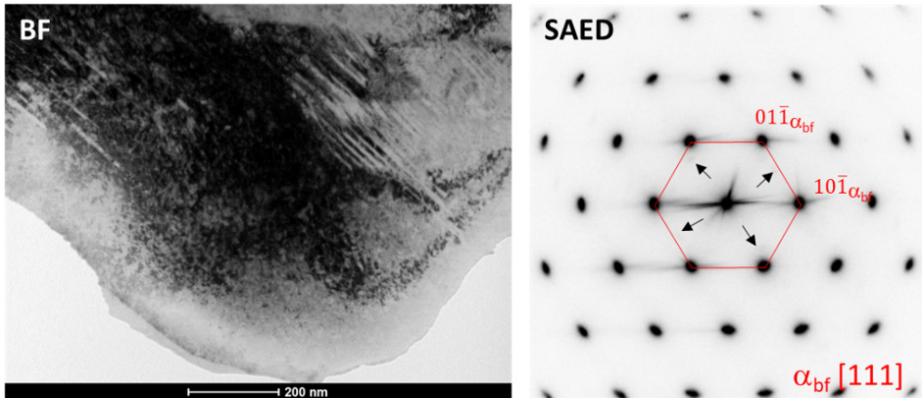

Fig. 8. BF microstructure and the corresponding SAED pattern of bainitic ferrite a_{bf} observed in the sample CS1100

made to make HREM observations in this area of the sample. An additional advantage of the analysed area is its location on the edge of the sample, where it is the thinnest and most suitable for high-resolution studies. Fig. 9 depicts the HREM microstructure performed in the area shown in Fig. 8 and the corresponding FFT (Fast Fourier Transform) and IFFT (Inverse Fast Fourier Transform) images. The FFT image attached in the lower right corner of the HREM image shows electron diffraction, which in addition to strong reflections from bainitic ferrite α_{bf} with [111] zone axis also shows additional reflections. The analysis of a selected area (blue square) of the HREM microstructure, in which the change in the contrast of atomic planes is clearly visible, allowed for the identification with high accuracy of the Θ-type transition carbide with an orthorhombic structure, Pnma space group and lattice parameters a = 5.0, b = 6.74 and c = 4.52 Å described in [21]. It is visible that these are carbides with the size up to 15 nm and elongated shape due to the anisotropy of their growth direction [21]. It can be expected that the presence of these nanometric carbides also have a positive effect on the strength properties and abrasion resistance of the investigated cast steels.

The mechanical properties of the investigated cast steel after two types of heat treatment were determined using of hardness HV30 and tensile test. One can see (TABLE 2) that only small differences between the hardness of these two samples exist. However, with regard to other mechanical properties, there are clear differences.

This is most likely due to the different volume fractions of retained austenite after both heat treatment variants. As shown in TABLE 1, more retained austenite remained in the microstructure of samples heat-treated according to the CS650 variant (67.8 wt.% compared to 58.8 wt.% after the CS1100 variant). However, such austenite was characterized by a lower carbon concentration. This made it less stable and therefore more susceptible to the TWIP or TRIP effect, which contributes to improving both strength and plastic properties. Unfortunately, this research did not verify which of the above-mentioned mechanisms turned out to be decisive for the observed improvement in mechanical properties. Therefore, in order to verify this thesis, in the future it is planned to perform an additional EBSD analysis of the samples after the tensile test, close to the point of rupture. Generally, in the light of literature data concerning cast steel subjected to bainitic reaction [9-12] our results are located in the same level of strength but with better ductility.

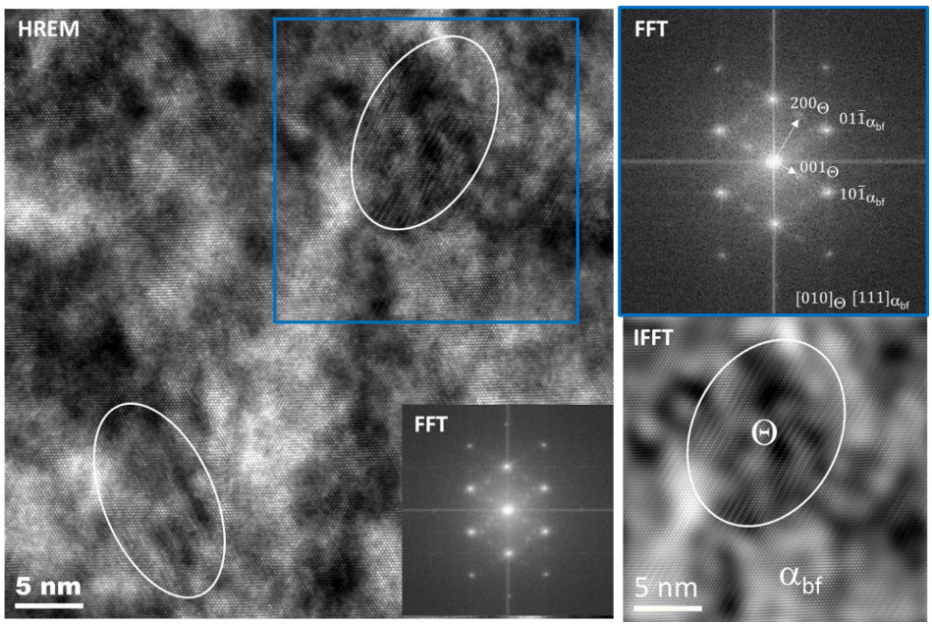

Fig. 9. HREM microstructure and corresponding FFT and IFFT images showing existence of Θ-type transition carbide in bainitic ferrite observed in the sample CS1100

TABLE 2

Mechanical properties of investigated cast steel measured by hardness and tensile test performed for three samples of each heat treatment

Sample	No	$HV30_{mean}$	R_m [MPa]	$R_{m\ mean}$ [MPa]	$R_{p0.2}$ [MPa]	$R_{p0.2\ mean}$ [MPa]	A [%]	A_{mean} [%]
CS650	1	658	1469	1426	1031	1060	9.5	9.5
	2		1410		1100		8.8	
	3		1399		1048		10.2	
CS1100	1	663	1438	1381	1041	992	8.2	8.5
	2		1292		963		9.3	
	3		1412		971		8.1	

4. Conclusions

In this work, we have developed two heat treatment technology variants and performed detailed microstructure, crystal structure and mechanical properties of cast steel with new chemical composition. It was shown that as a result of using two alternative variants of multi-stage heat treatment for investigated cast steel, the microstructures produced consisted of martensite plates with a width of 200 to 500 nm and retained austenite with a width of a dozen to 50 nm for variant 1 and from several dozen to 200 nm for variant 2, which were related to Kurdiumov-Sachs crystallographic relationship. Both microstructures also contained nanometric-size (~15 nm) of Θ-type transition carbides. The volume fraction of retained austenite and martensite varied depending on the heat treatment used and these values were 67.8 and 32.2% for variant 1 and 58.8 and 41.2% for variant 2, respectively. The main reason for these differences was dendritic segregation causing the change of chemical composition of austenite formed at 950°C and, consequently, different mechanical stability of this phase. Mechanical properties determined during tensile tests showed that the tensile strength and ultimate tensile strength for variant 1 was R_m = 1426 MPa and $R_{0,2}$ = 1060 MPa and for variant 2 R_m = 1381 MPa and $R_{0,2}$ = 992 MPa, with the elongation to break the sample A = 9.5 and A = 8.5%, respectively. These values of strength are slightly lower than presented in literature for this type of cast steel but ductility is significantly better. The developed cast steel has great application potential, in particular for applications such as materials with high abrasion resistance due to the type of microstructure.

Acknowledgements

The research was co-financed by the Polish Ministry of Science and Higher Education in the frame of the project DWD/3/29/2019 “Doktorat Wdrożeniowy”. The research was supported by National Centre for Research and Development, Poland in frame of “Szybka Sciezka” program, project title: “Development and implementation of an innovative technology for casting of thin-walled elements based on Fe matrix for defence and automotive industries characterized by high dimensional accuracy and increased strength” project number: POIR.01.01.01-00-0197/17.

REFERENCES

[1] F.G. Caballero, H.K.D.H. Bhadeshia, K.J.A. Mawella, D.G. Jones, P. Brown, Mater. Sci. Technol. **18**, 279 (2002).
[2] B. Avishan, S. Yazdani, F.G. Caballero, T.S. Wang, C. Garcia-Mateo, Mater. Sci. Technol. **31**, 1508 (2015).
[3] A. Kapito, R.J. Mostert, W.E. Stumpf, C.W. Siyasiya, IOP Conf. Ser.: Mater. Sci. Eng. **655**, 012012 (2019).
[4] V. Efremenko, O. Hesse, Thalmann Friedrich, M. Kunert, M. Brykov, K. Shimizu, V. Zurnadzhy, P. Suchmann, Wear **418-419**, 24 (2019)
[5] N. Fonstein, Springer, ISBN 978-3-319-19165-2 (eBook) (2015).
[6] M. Franceschi, L. Pezzato, C. Gennari, A. Fabrizi, M. Polyakova, D. Konstantinov, K. Brunelli and M. Dabalà, Metals **10**, 1448 (2020)
[7] M. Franceschi, C. Soffritti, A. Fortini, L. Pezzato, G.L. Garagnani, M. Dabalà, Tribology International **178**, 108071 (2023).
[8] L.C Chang, Wear **258**, 730 (2005).
[9] A.F. Santacruz-Londoño, O. Rios-Diez, J.A. Jiménez, C. Garcia-Mateo, R. Aristizábal-Sierra, Metals **10**, 612, (2020).
[10] N.E. Tenaglia, J.M. Massone, R.E. Boeri, J.G. Speer, Mater. Sci. Tech. **36**, 690 (2020).
[11] A. Basso, A. Eres-Castellanos, N. Tenaglia, D. San-Martin, J.A. Jimenez, F.G. Caballero, Metals **11**, 220 (2021).
[12] E. Skołek, K. Szwejkowska, K. Chmielarz, W.A. Świątnicki, D. Myszka, A.N. Wieczorek, Metallurgical and Materials Transactions **A 53**, 2544 (2022)
[13] M. Zhou, G. Xu, H. Hu, Q. Yuan, J. Tian, Materials Science & Engineering **A 704**, 427 (2017).
[14] C. Garcia-Mateo, J.A. Jimenez, H.-W. Yen, M.K. Miller, L. Morales-Rivas, M. Kuntz, S.P. Ringer, J.-R. Yang, F.G. Caballero, Acta Materialia **91**, 162 (2015).
[15] Q. Luo, Journal of Materials Engineering and Performance **25**, 2170 (2001).
[16] S. Curtze, V.-T. Kuokkala, Acta Materialia **58**, 5129 (2010).
[17] N.E. Tenaglia, J.M. Massone, R.E. Boeri, J.G. Speer, Mater. Sci. Tech. **36**, 690 (2020).
[18] Hong-Seok Yang, H.K.D.H. Bhadeshia, Scripta Materialia **60**, 493-495 (2009).
[19] Anže Bajželj, Jaka Burja, Crystals **12**, 1449 (2022).
[20] W. Gong, Y. Tomota, S. Harjo, Y.H. Su, K. Aizawa, Acta Materialia **85**, 243 (2015).
[21] Y. Kawahara, K. Kaneko, H. Sawada, J. Takahashi, Acta Materialia **252**, 11891, (2023).